Supplementary Information

Structure-toxicity Relationship in Intermediate Fibrils from α-Synuclein Condensates

Serene W. Chen[†], Joseph D. Barritt[†], Roberta Cascella, Alessandra Bigi, Cristina Cecchi, Martina Banchelli, Angelo Gallo, James A. Jarvis, Fabrizio Chiti, Christopher M. Dobson, Giuliana Fusco[*] and Alfonso De Simone[*]

[†] These authors contributed equally to this work

*Alfonso De Simone and Giuliana Fusco
Emails: alfonso.desimone@unina.it and gf203@cam.ac.uk

This PDF file includes:

Figures S1 to S16
Tables S1 to S3
SI References

SI Figures

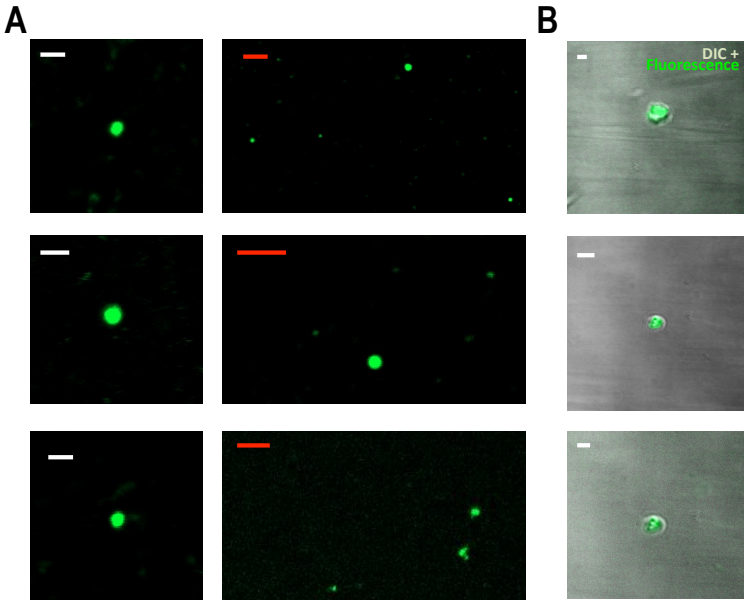

Figure S1. Gallery of confocal microscopy and DIC images of αS spherical condensates. The condensates readily form at 37 °C at the incubation conditions utilized in this study. The condensates present a round shape and liquid-like properties (Fig. S2). The present images were measured using fluorescently labeled αS samples (using 1% of AF488-αS_{N122C}). **A)** Gallery of confocal microscope images of spherical αS condensates. Scale bars of 1µm (white) and 5µm (red). **B)** Differential Inference Contrast (DIC) microscopy images merged with fluorescence confocal microscopy images of large αS condensates (scale bar 1µm).

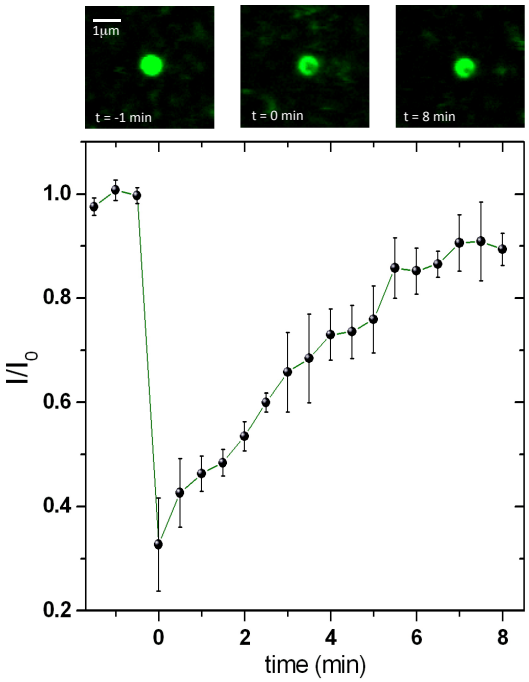

Figure S2. Fluorescence recovery after photobleaching (FRAP) experiments. (top) Fluorescently labeled condensate of αS (1% of AF488-αS_{N122C}) prior bleaching (left), immediately after bleaching (centre) or after 8 min after bleaching (right) the bleaching show the liquid like properties of the condensate (scale bar 2µm). (bottom) Analysis of the fluorescence intensity in the ROI (*I*) during the FRAP experiments. Error bars from triplicates.

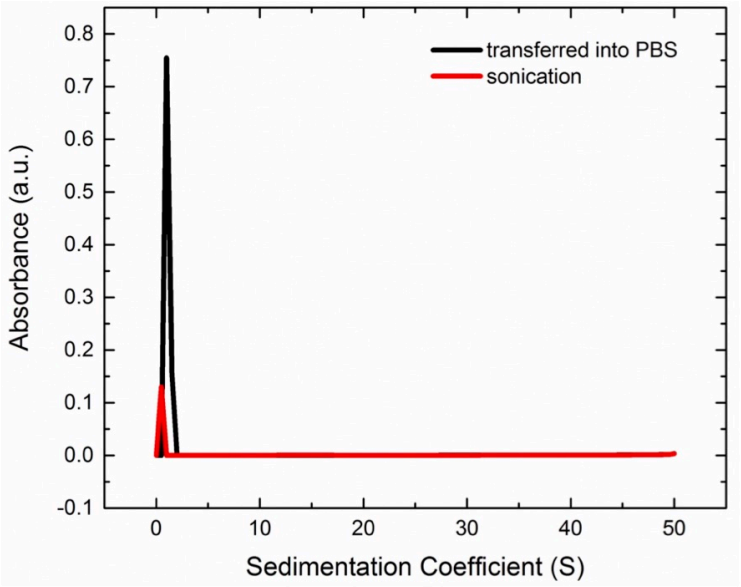

Figure S3. Liability of the *early-fibrils* from αS condensates. Sedimentation coefficients of the *early-fibrils* measured using analytical ultracentrifugation. The measurement indicates that the fibrils disassemble into monomers as a result of sonication (red) or transfer into PBS for 24h (black), with no presence of detectable oligomers.

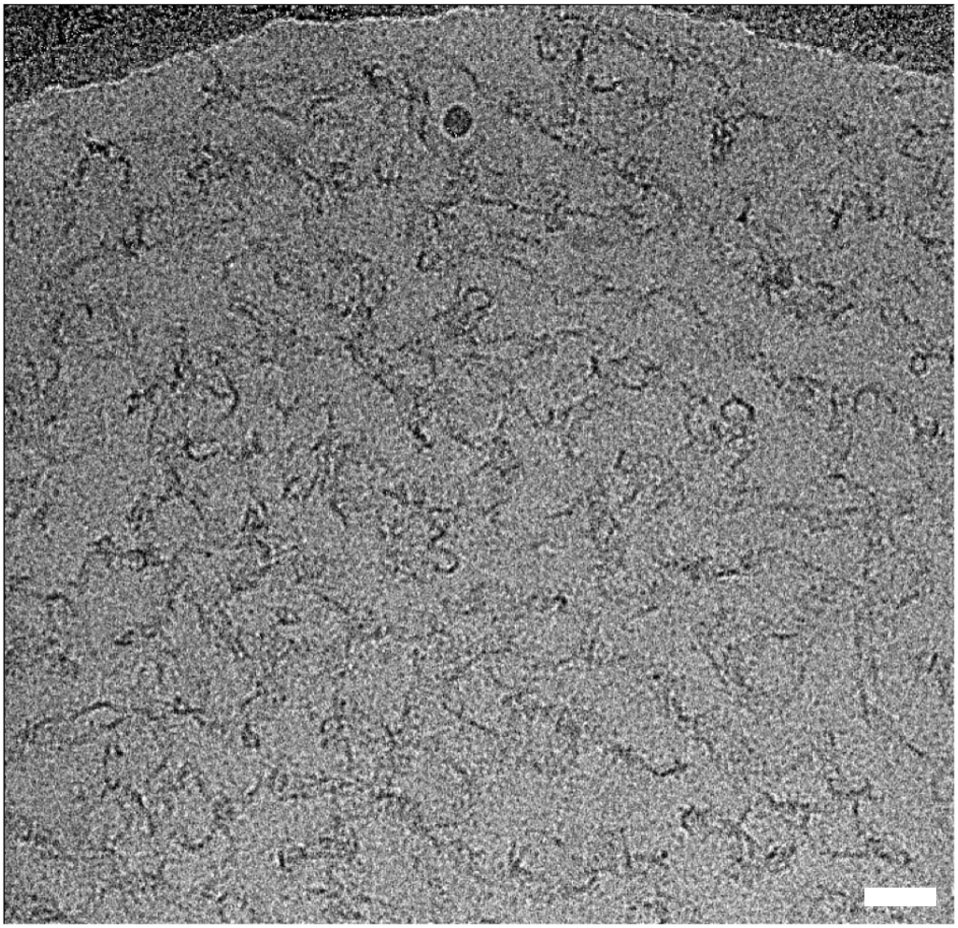

Figure S4. CryoEM micrograph of *early-fibrils* from αS condensates. Representative micrograph of early-fibrils measured using Titan Krios 300 kV microscope with Falcon III detector. Scale bar 200 nm.

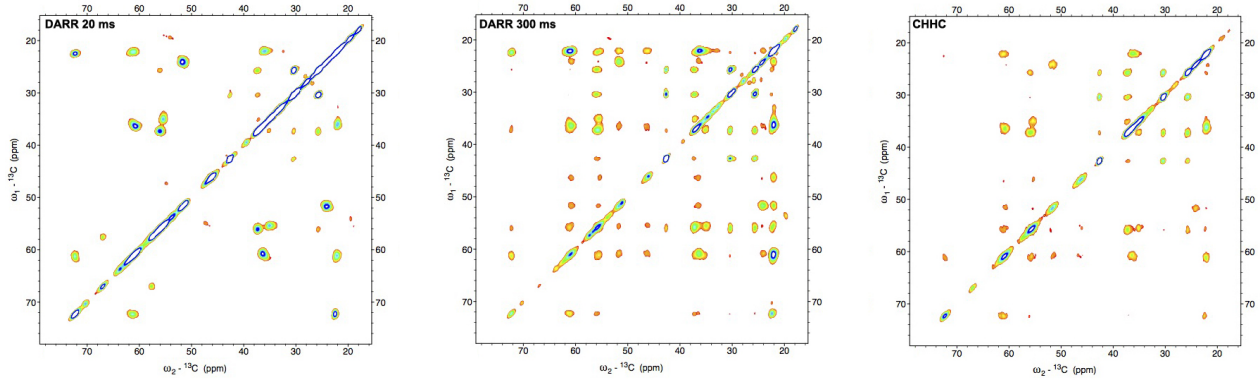

Figure S5. DARR and CHHC spectra of *early-fibrils* from αS condensates. Core regions of the *early-fibrils* probed using CP MAS ssNMR. The acquisition of well resolved CP MAS spectra, as here shown in the examples of DARR[1] (mixing times of 20 and 300 ms) and CHHC spectra,[2] indicates that the *early-fibrils* are relatively homogeneous in the local structure of the core regions. By contrast, the variety of curvatures in the fibrils stretches had likely a negative impact on single particle analysis of the cryo-EM data.

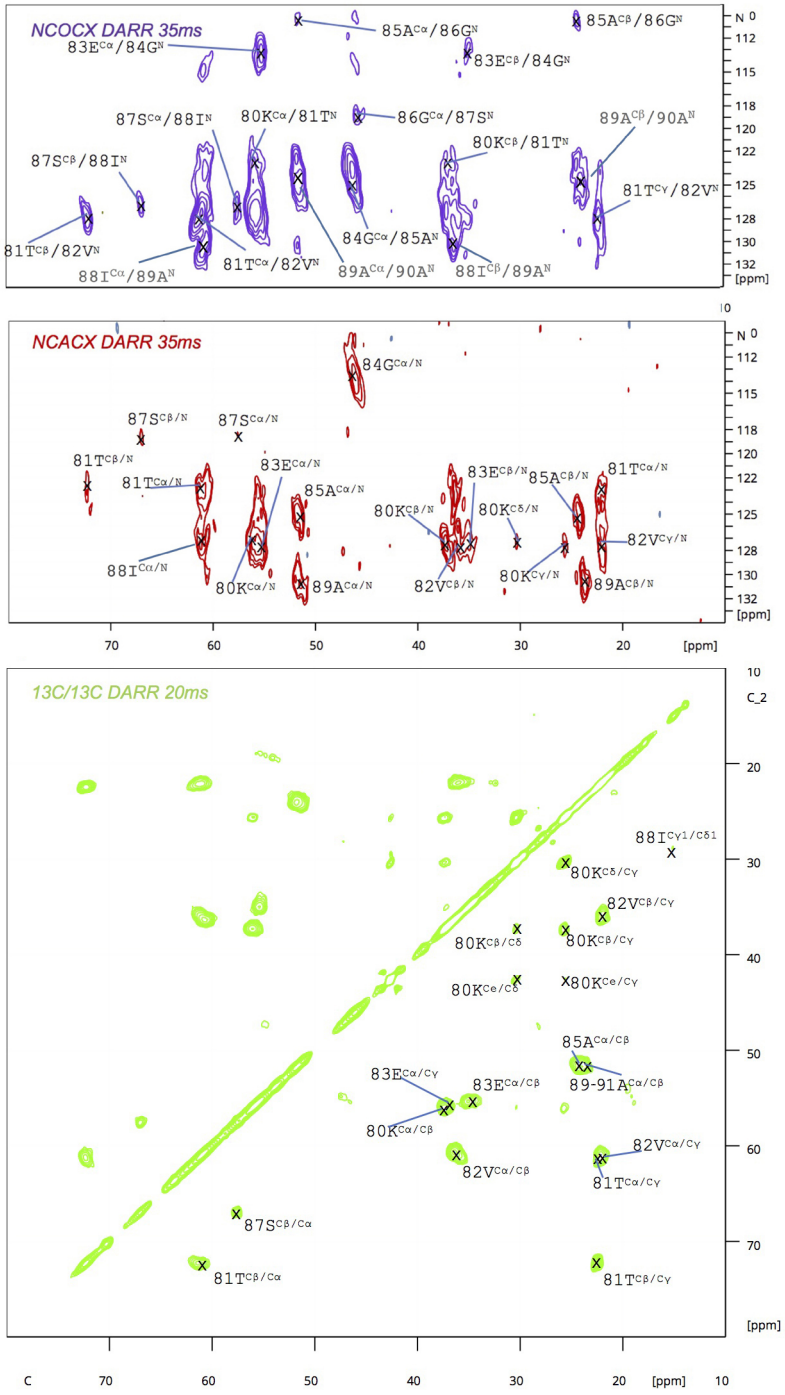

Figure S6. Assignment of the ssNMR resonances of the *early-fibrils* of αS. The resonances of the MAS ssNMR ^{13}C-^{13}C DARR spectra of the *early-fibrils* were assigned by means of a combination of NCACX and NCOCX. While the DARR spectra showed relatively sharp ^{13}C resonances, these intermediate fibrils were found to posses faster transverse relaxation in the ^{15}N nuclei, resulting in broader resonances on these nuclei. Despite the broad nature of ^{15}N resonances, the combination of NCACX and NCOCX identified unambiguous pairs of consecutive residues, including TV, EG, AG, GA, SI, AA, and IA. These pairs are all simultaneously present in one single region of the protein, namely the fragment 80-KTVEGAGSIAAA-91. A vertical stack of NCOCX, NCACX and DARR (20 ms mixing time) is shown. These data were verified using 3D versions of (NCOCX and NCACX).

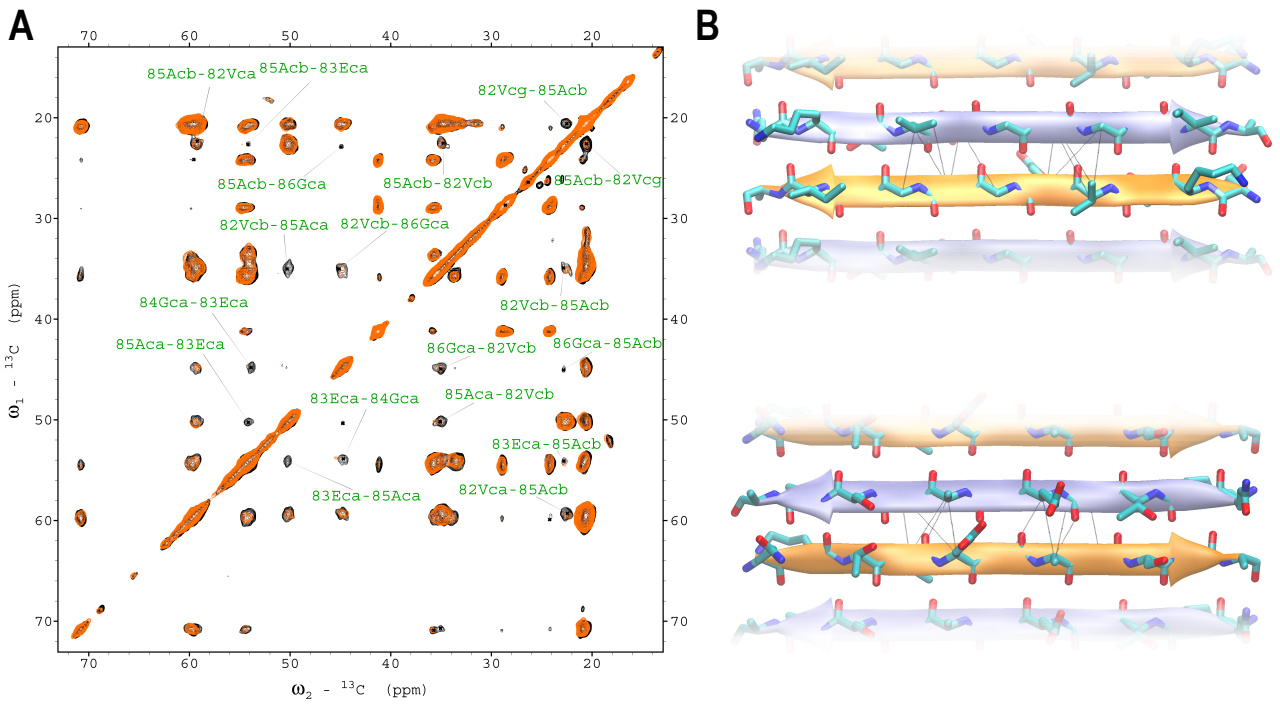

Figure S7. Intermolecular contacts in *early-fibrils* from αS condensates probed using 300 ms ^{13}C-^{13}C DARR ssNMR. A) Overlay of ^{13}C-^{13}C DARR ssNMR spectra of *early-fibrils* measured with a mixing time of 300 ms. Black spectrum: ^{13}C fully-labelled; Orange spectrum: 50:50 ^{13}C:^{12}C mixed-labelled. Some cross-peaks in the ^{13}C fully-labelled spectrum cannot be associated to local contacts in the αS sequence. The reduced signal-to-noise of these peaks in the mixed-labelled sample, however, indicates that they arise from inter-molecular contacts across β-strands. **B)** Structural model of the β-sheet based on the intermolecular contacts identified in the 300ms DARR in the fragment 80-KTVEGAGSIAAA-91. The ssNMR-informed modelling was consistent with an antiparallel topology revealing an asymmetric distribution of the side chains in the β-sheet, with one surface presenting mainly hydrophobic side chains (top) and the opposite showing mostly hydrophilic side chains (bottom).

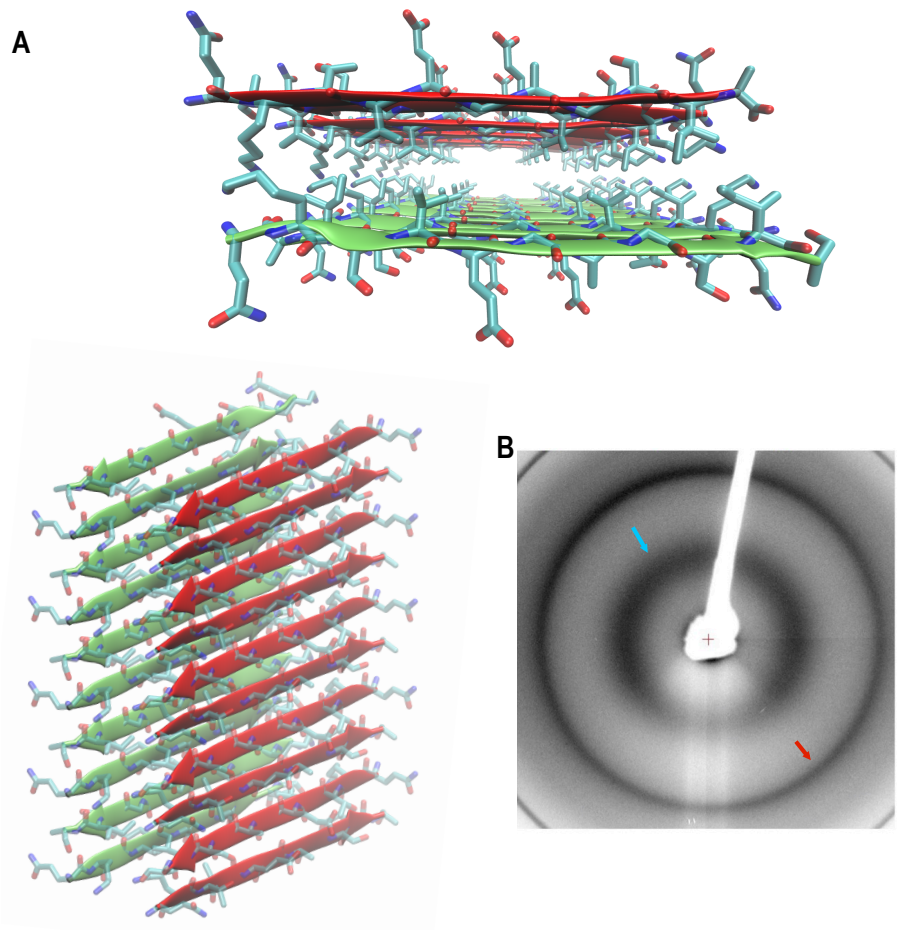

Figure S8. Model of the fibril core of the *early-fibrils* of αS from sparse biophysical data. A) Starting from the model of the antiparallel β-sheet unit (Fig. S7), it was possible to generate a model of the stack of two β-sheets using the information of the un-oriented X-ray diffraction pattern (**B**), showing a reflection at 10 Å (cyan arrow). The model suggests that the fragment 80-KTVEGAGSIAAA-91 can generate a β-sheet stacking with a hydrophobic core, stabilized by bulky residues such as Val and Ile, and hydrophilic side chains pointing toward the solvent. The presence of Gly residues in the β-sheet stack may provide these transient aggregates with the structural plasticity to allow for the variety of curvatures observed in cryo-EM analyses (Fig. S4 and 3A).

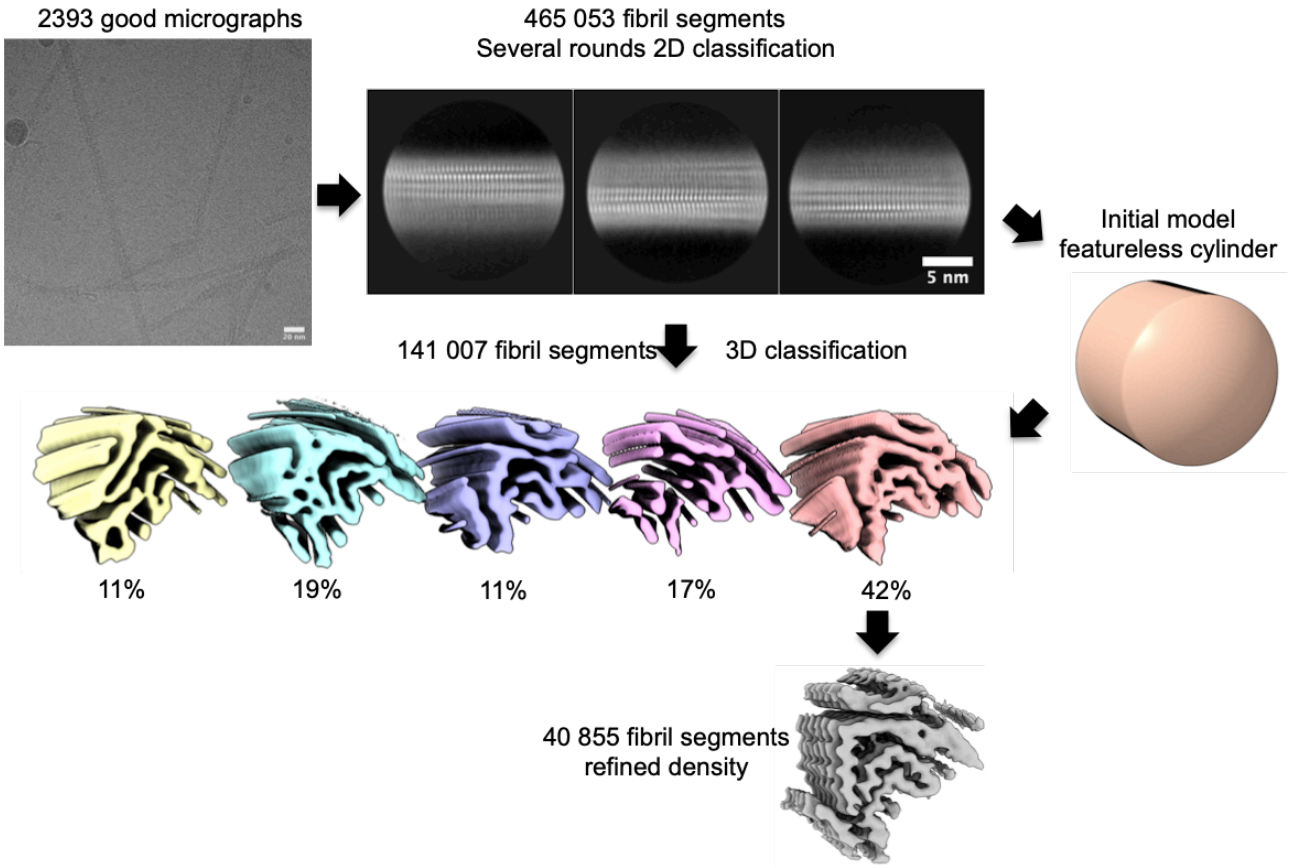

Figure S9. Helical reconstruction of the *late-fibrils* structure from cryo-EM images. Raw cryo-EM micrographs of the *late-fibrils* measured with a Titan Krios 300 kV microscope were processed into 2D class averages. Several rounds of 2D classification were used to select the best particles for 3D reconstruction. Successive rounds of 3D classification further removed noisy or ambiguous fibril segments. The final refined helical reconstruction was filtered with a B-factor of -200 using post-processing.

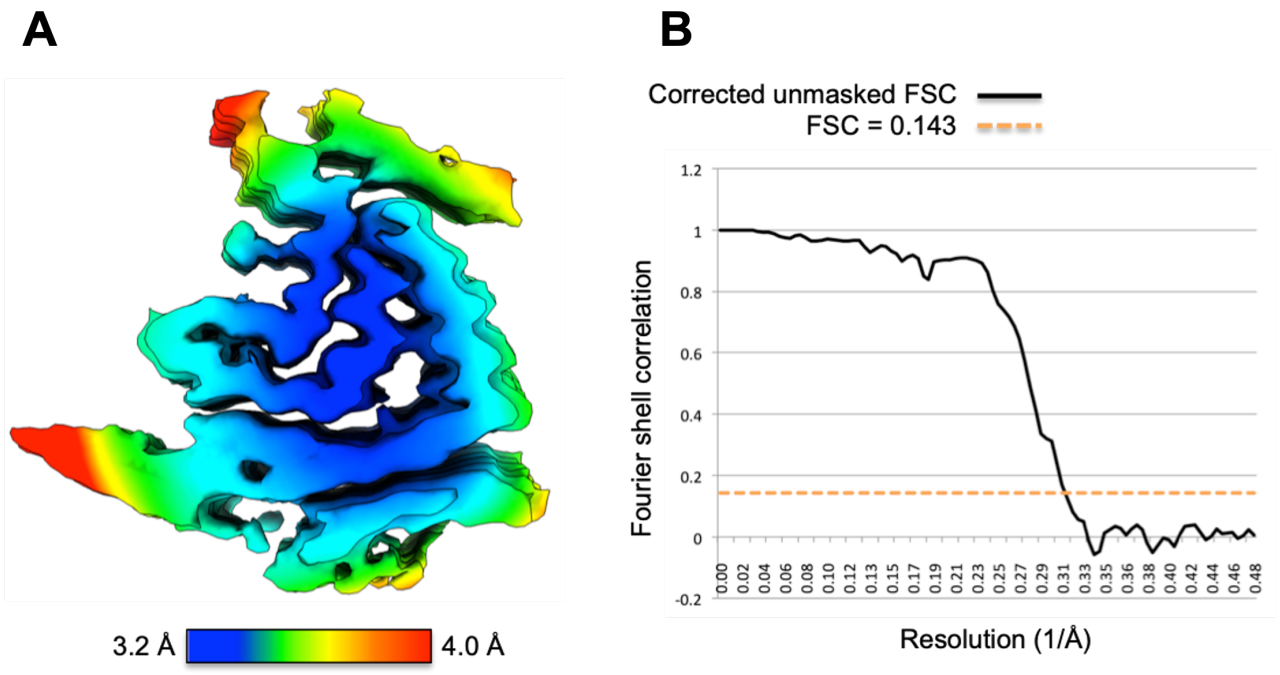

Figure S10. Resolution estimates of the final EM density map of the *late-fibrils.* The local resolution of the final sharpened map ranges from 3.2 (blue) to 4.0 Å (red) highlighted by a heat map in A. The Fourier shell correlation curve for the same masked density from A with a global resolution of 3.3Å at a cutoff of FSC = 0.143.

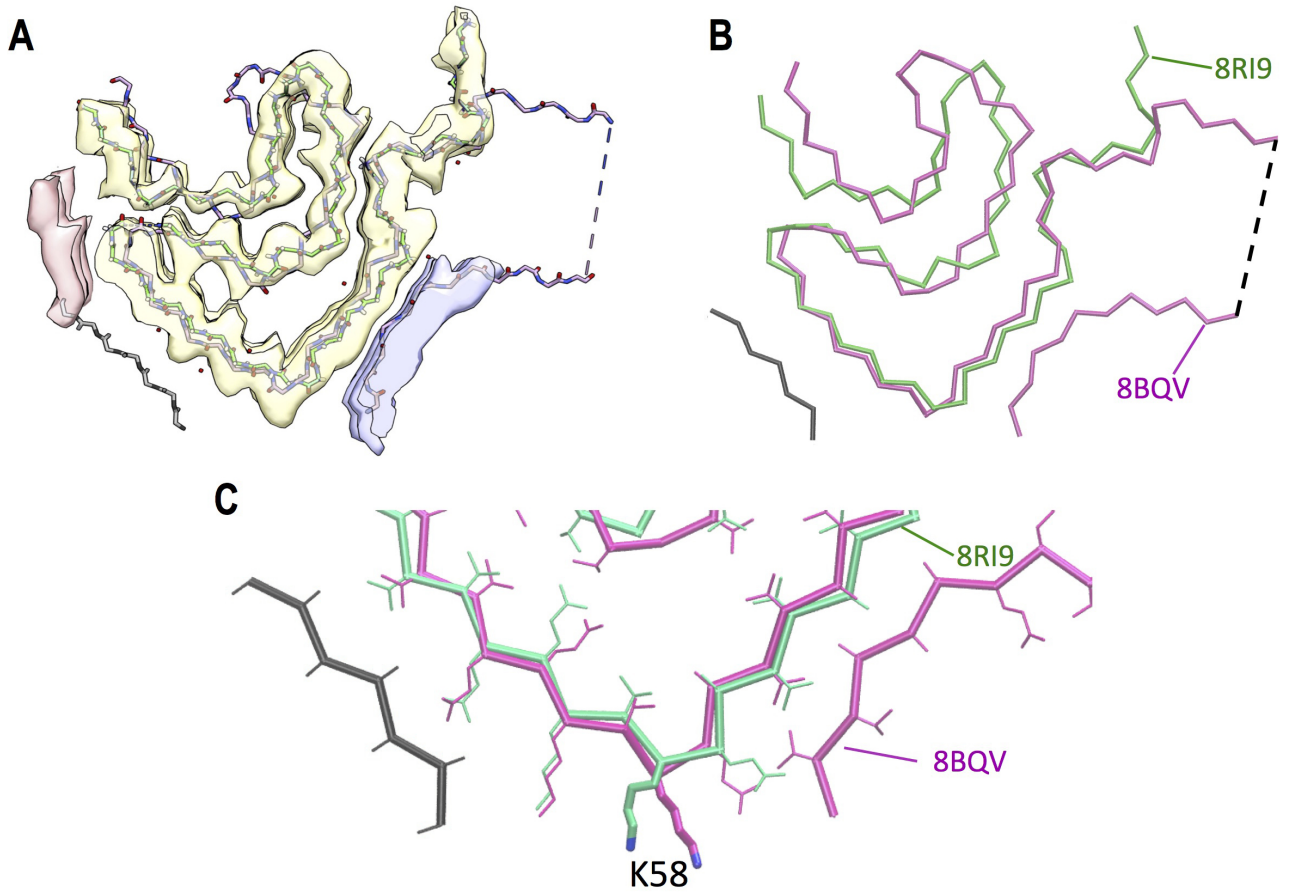

Figure S11. Structural superimposition between the structure of juvenile-onset synucleinopathy (JOS) fibrils of αS and the *late-fibrils* from condensates. Backbone atoms of *late-fibrils* from αS condensates (PDB code: 8RI9) and JOS singlet fibrils[3] (PDB code: 8BQV) are shown in green and purple, respectively (all panels). **A**) 8RI9 peptide backbone fitted into the *late-fibril* EM density (EMD-19184) with 8BQV aligned with respect to 8RI9. The resolution of two regions of the density map (colored in purple and pink) was too low to enable model building, however, the overlay with JOS fibrils[3] suggests that one of these regions (purple density) can be attributed to the N-terminal region of αS structured around the core of the fibril. The JOS structure[3] also reported an unknown peptide density modelled as polyalanine (grey). **B**) Backbone trace alignment of 8RI9 (purple) and 8BQV (green). The RMSD between the structures (calcualted using Cα atoms of residues 41 to 98) is 4.3 Å. **C)** Local alignment of the most similar regions, spanning residues 41 to 66 (RMSD on Cα atoms of 1.12 Å) and comprising the first two β-strands of the core. There is a close match between the two structures in this region, including the topology of Lys 58, which points outward in both assemblies.

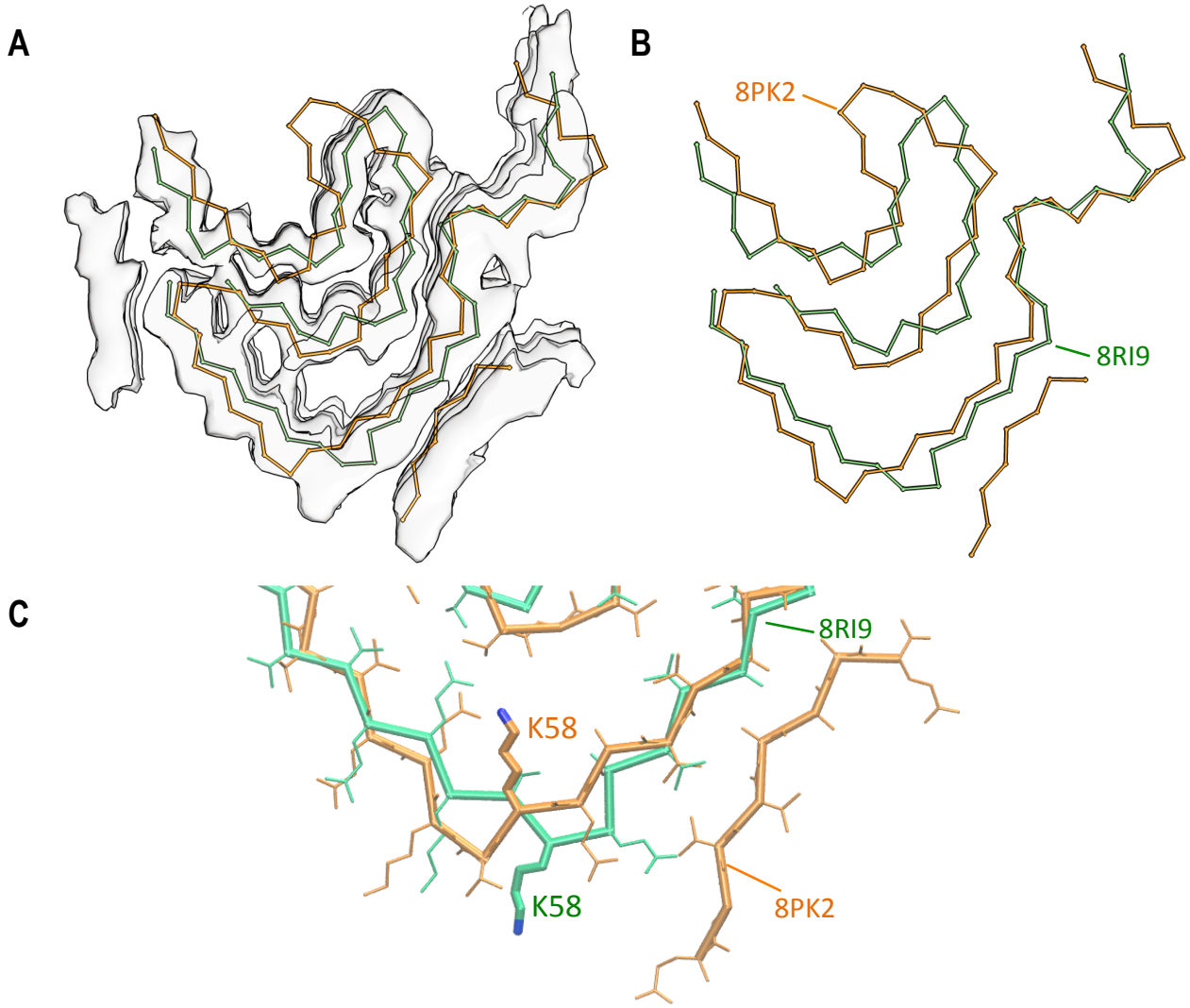

Figure S12. Structural superimposition between the 1M monofilament polymorph observed *in vitro* at pH 7.0 [4] and the *late-fibrils* from αS condensates. A) Cα-trace fitted into the *late-fibril* EM density (EMD-19184) with 8PK2 aligned with respect to 8RI9 by considering the Cα atoms of residues 41 to 97 only. *late-fibril* (PDB code: 8RI9) and 1M filament [4] (PDB code: 8PK2) are shown in green and orange, respectively (all panels). **B**) Backbone traces as in panel A. The RMSD between the structures (calculated using Cα atoms of residues 41 to 97) is 4.63 Å. **C)** Local alignment of the region spanning residues 41 to 66 (RMSD on Cα atoms of 2.34 Å) and comprising the first two β-strands of the core. In this case, Lys 58 points outward in the *late-fibrils* and inward in the 1M. The observation that the *late-fibrils* adopt a monofilament topology at pH 7.4 suggests the possibility of a local lowering of the pH within the αS condensates, as *in vitro* the 1M polymorphism has been shown to occur at pH 7.0.[4]

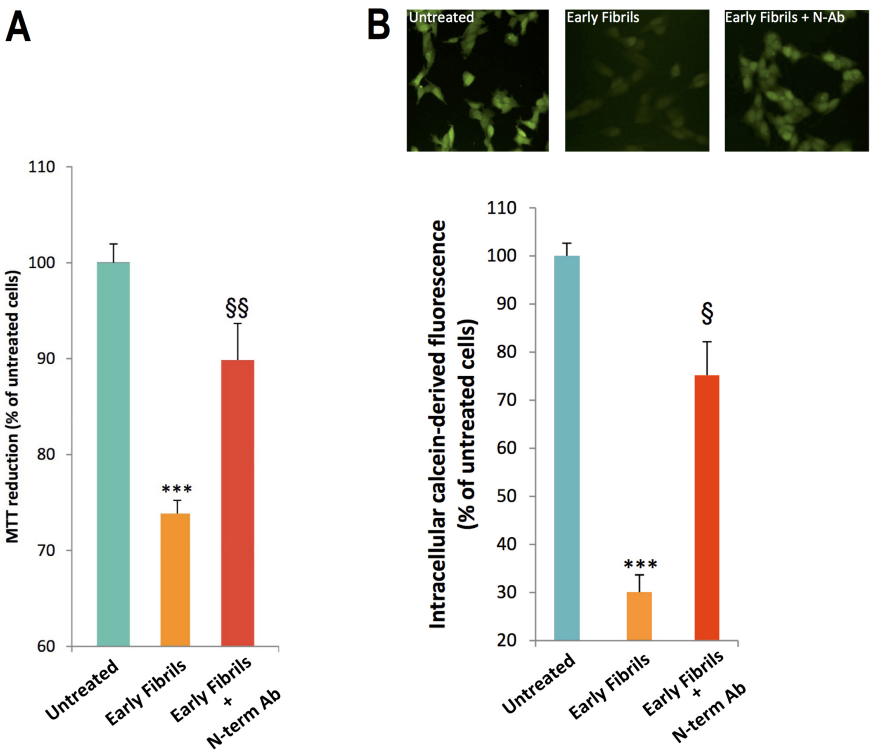

Figure S13. Suppression of the cytotoxicity of the early-fibrils of αS upon binding of the N-terminal antibody. A) Cell dysfunction monitored by the reduction of MTT in human neuroblastoma SH-SY5Y upon incubation with 0.3 μM (monomer equivalents) of *early-fibrils* from αS condensates, and in the presence or absence of equimolar amounts of N-terminal antibody. **B)** Cell dysfunction monitored by intracellular ROS production in human neuroblastoma (details as in panel A). *** indicates a P value < 0.001 with respect to untreated cells. § and §§ indicate P values respectively < 0.01 and < 0.05 with respect to cells treated with *early-fibrils* (0.3 μM monomer equivalents).

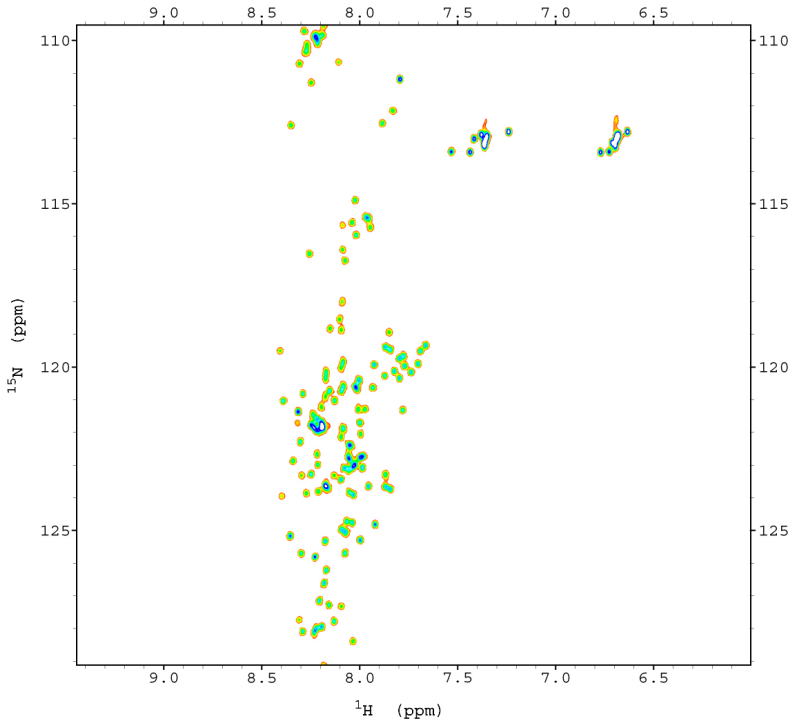

Figure S14. ^{1}H-^{15}N HSQC spectrum of αS monomers under conditions promoting self-assembly in liquid-like spherical condensates. The spectrum was recorded at 283 K at a ^{1}H frequency of 700 MHz, using a protein concentration of 100 μM.

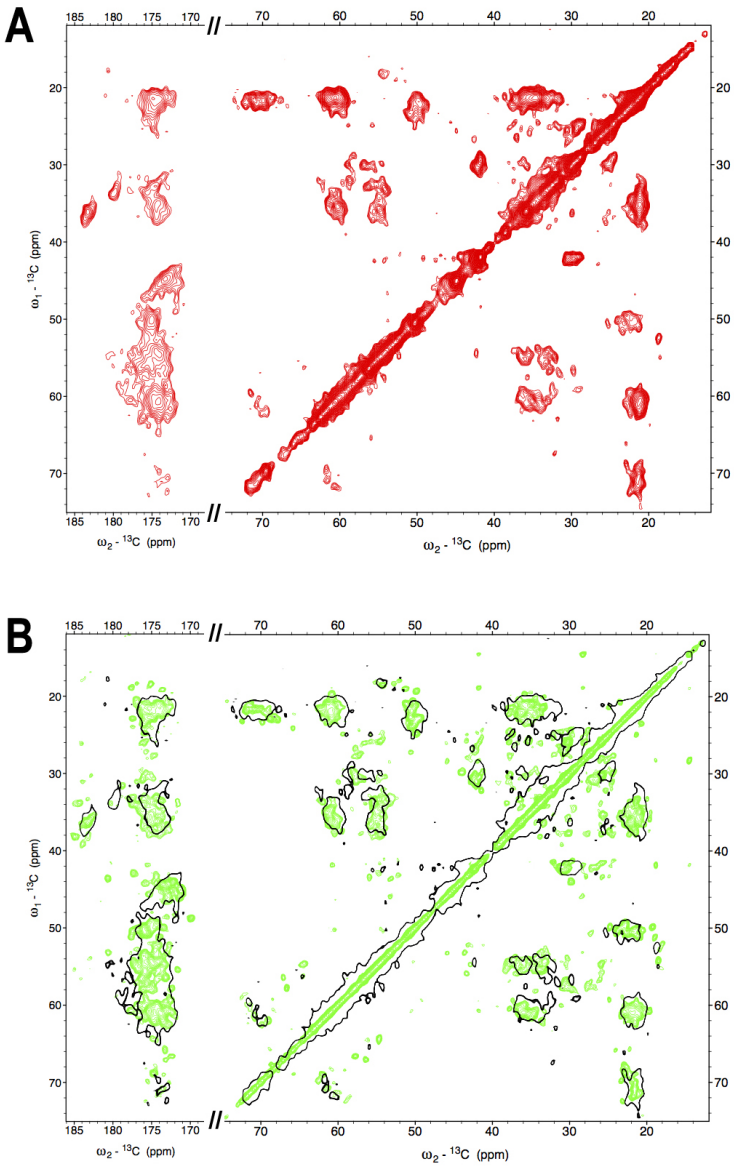

Figure S15. ^{13}C-^{13}C DARR spectra of *late-fibrils* of αS. A) ^{13}C-^{13}C DARR correlation spectrum (aliphatic and carbonyl regions) of the *late-fibrils* of αS after 3 weeks of incubation (standard *late-fibrils*). Prior the packing into 3.2 mm ssNMR rotor, the fibrils were pelleted and resuspended in PBS for 24h at 37°C. ssNMR spectra were acquired at 25°C using 20 ms of mixing time and 1 ms of contact time and a MAS rate of 12.5 kHz. **B)** ^{13}C-^{13}C DARR spectra of standard *late-fibrils* (black) and seeded *late-fibrils* (green). The seeded *late-fibrils* were obtained using seeds from the sonicated standard *late-fibrils* (1 min sonication using a Bandelin Sonopuls HD2070 sonicator with 30% cycles at 10% maximum power). The sonicated fibrils were incubated with fresh monomers at 37°C overnight (with seeds representing 10% of αS) at a total protein concentration of 100 µM in PBS and 0.02% sodium azide. For clarity, the spectrum of standard *late-fibrils* is shown as a single black contour line. The seeded fibrils show essentially the same spectrum of the standard *late-fibrils*, but with better signal to noise and improved line widths of the resonances, thus enabling the assignment of the peaks.

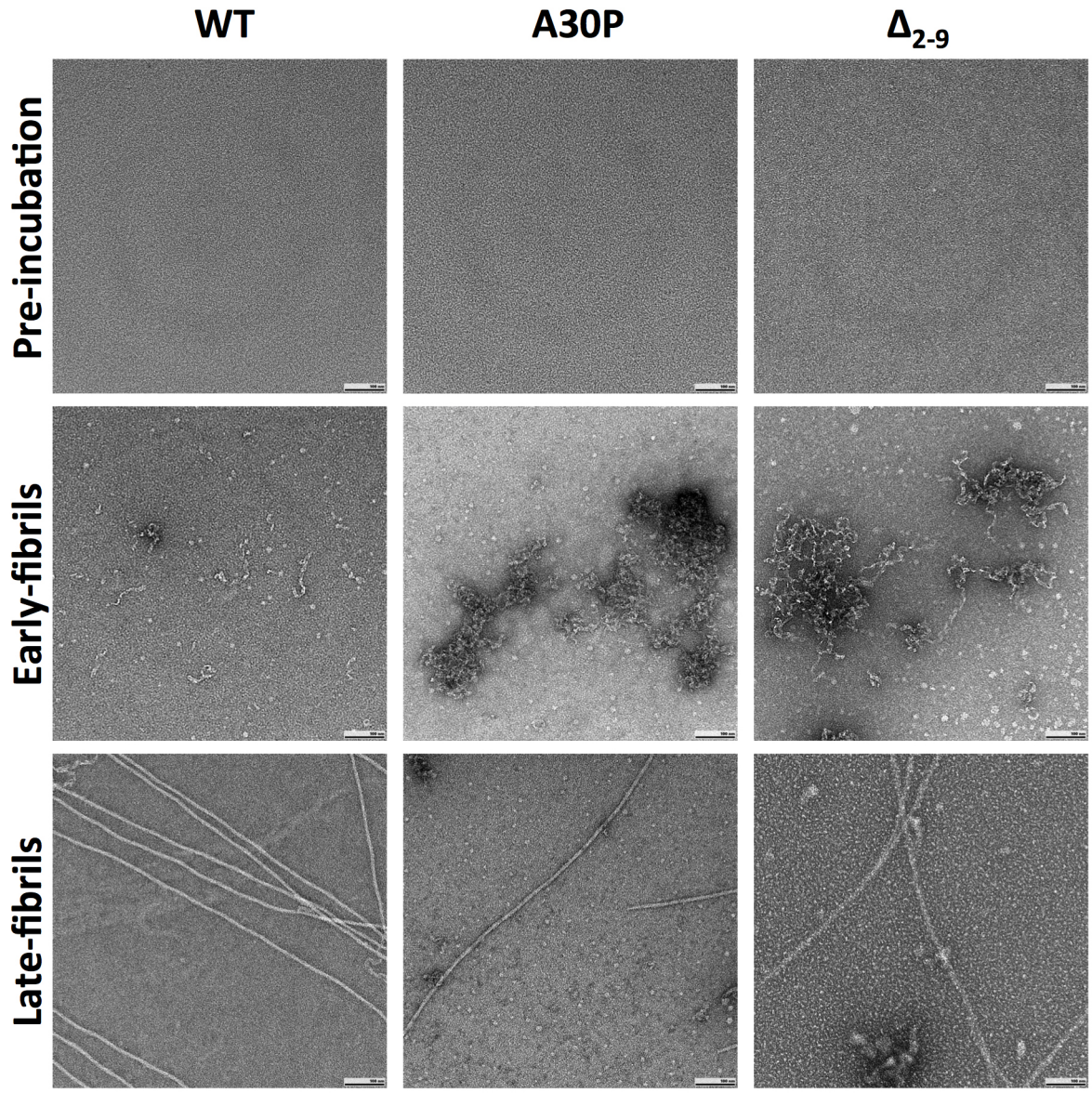

Figure S16. *Early*- and *late-fibrils* with A30P and Δ_2-9 mutants of αS. Negatively stained TEM micrographs of a time-course showing pre-incubation, *early-fibrils* and *late-fibrils* of wild-type αS (left column), A30P mutant αS (middle column) and Δ_{2-9} αS (right column). Scale bars are 100 nm in length.

Table S1. MAS ssNMR Chemical shifts of early-fibrils core

Residue nr.	Residue name	Atom Type	Chemical Shift (ppm)
80	LYS	C	175.1
80	LYS	CA	56
80	LYS	CB	37.4
80	LYS	CD	30.4
80	LYS	CE	42.7
80	LYS	CG	25.8
80	LYS	N	127.5
81	THR	C	174.0
81	THR	CA	61.4
81	THR	CB	72.3
81	THR	CG	22.4
81	THR	N	122.5
82	VAL	C	174.4
82	VAL	CA	60.7
82	VAL	CB	36.1
82	VAL	CG%	21.9
82	VAL	N	127.8
83	GLU	C	175.5
83	GLU	CA	55.4
83	GLU	CB	35.1
83	GLU	CD	183.0
83	GLU	CG	37.1
83	GLU	N	127.6
84	GLY	C	172.1
84	GLY	CA	46.3
84	GLY	N	113.1
85	ALA	C	176.2
85	ALA	CA	51.7
85	ALA	CB	24.3
85	ALA	N	125.1
86	GLY	C	172.1
86	GLY	CA	46.0
86	GLY	N	110.5
87	SER	C	173.5
87	SER	CA	57.6
87	SER	CB	67.0
87	SER	N	118.7
88	ILE	CA	61.2
88	ILE	CB	36.8
88	ILE	CD1	15.0
88	ILE	CG1	28.8
88	ILE	N	126.8
89	ALA	C	176.2
89	ALA	CA	51.5
89	ALA	CB	23.6
89	ALA	N	130.8
90	ALA	N	125.0

Table S2. CryoEM data collection parameters

Data collection parameters	
Microscope	Titan Krios
KeV	300
Camera	Falcon III
Collection mode	Counting mode
C2 aperture (µm)	50
Objective aperture (µm)	70
Nominal magnification	120 000
Pixel size (Å)	1.043
Number of frames	38
Dose rate ($e^-/Å^2/s$)	1.075
Total dose ($e^-/Å^2$)	43
Defocus range (µm)	-0.9 to -3.0
Number of micrographs	3262

Table S3. CryoEM Helical Reconstruction

Data processing statistics	
Initial fibril segment number	465 053
Final particle number	141 007
Symmetry imposed	C1
Global map resolution (Å) FSC = 0.143	3.4
Local resolution range (Å)	3.2 – 4.0

SI References

1. Takegoshi, K.; Terao, T., 13C-1H dipolar recoupling under very fast magic-angle spinning using virtual pulses. *Solid state nuclear magnetic resonance* **1999,** *13* (4), 203-12.
2. Lange, A.; Becker, S.; Seidel, K.; Giller, K.; Pongs, O.; Baldus, M., A concept for rapid protein-structure determination by solid-state NMR spectroscopy. *Angewandte Chemie* **2005,** *44* (14), 2089-92.
3. Yang, Y.; Garringer, H. J.; Shi, Y.; Lövestam, S.; Peak-Chew, S.; Zhang, X.; Kotecha, A.; Bacioglu, M.; Koto, A.; Takao, M.; Spillantini, M. G.; Ghetti, B.; Vidal, R.; Murzin, A. G.; Scheres, S. H. W.; Goedert, M., New SNCA mutation and structures of α-synuclein filaments from juvenile-onset synucleinopathy. *Acta neuropathologica* **2023,** *145* (5), 561-572.
4. Frey, L.; Ghosh, D.; Qureshi, B. M.; Rhyner, D.; Guerrero-Ferreira, R.; Pokharna, A.; Kwiatkowski, W.; Serdiuk, T.; Picotti, P.; Riek, R.; Greenwald, J., On the pH-dependence of α-synuclein amyloid polymorphism and the role of secondary nucleation in seed-based amyloid propagation. *eLife* **2024,** *doi:10.7554/eLife.93562.1.sa3*.